Frequency Shifter-RIS Assisted Standalone mmWave Cellular Networks

Chen Hu, Kun; Williams, Robin Jess; Alù, Andrea; Popovski, Petar

Published in:
IEEE Transactions on Wireless Communications

DOI (link to publication from Publisher):
10.1109/TWC.2024.3385023

Publication date:
2024

Document Version
Accepted author manuscript, peer reviewed version

Frequency Shifter-RIS Assisted Standalone mmWave Cellular Networks

Kun Chen-Hu, *Member, IEEE*, Robin J. Williams, *Student Member, IEEE*, Andrea Alù, *Fellow, IEEE*, and Petar Popovski, *Fellow, IEEE*

***Abstract*—Frequency shifting-reconfigurable intelligent surfaces (FS-RISs) can be built by a new generation of meta-materials and circuits, which can perform an operation that changes the original frequency spectrum of the transmitted signal. Its exploitation for wireless communications is still in its infancy. In this work, a millimetre wave (mmWave) cellular network aided by FS-RIS is proposed to satisfy the new challenging communication services. The FS-RIS is able to down-convert the carrier frequency of the mmWave signal and spread the control information to the cell by using a more reliable and stable link, relying on better propagation within the lower bands, and a novel multi-frequency beam-management procedure is given. The proposed method can rapidly discover all users in the entire cell by using different sizes of beams. It avoids range penalization due to the better propagation in sub-6 GHz bands, unlike the hierarchical BMP. Additionally, the proposed technique only requires one base station (BS), and hence the delay overhead caused by the information exchange among several BSs is fully avoided, unlike the case of coordinated multi-point (CoMP). Overall, this paper provides a new way to exploit FS-RIS in wireless systems, which can potentially change the way we look at spectrum and interference management for the efficient exploitation of communication applications.**

***Index Terms*—beam-management, frequency shifting, meta-surface, mmWave, RIS.**

I. Introduction

NEW services based on enhanced mobile broadband (eMBB) under mobility scenarios is a key target in the evolution from current Fifth Generation (5G) [1] to the next Sixth Generation (6G) [2]–[4] of cellular networks. Applications based on extended reality [4] will require a huge amount of spectrum resources is a must. Therefore only available at higher frequency bands, such as millimetre waves (mmWave) [3] since the traditional sub-6 GHz band is already extremely saturated. Moreover, large antenna arrays can be exploited due to the shorter wavelengths, which implies using very narrow directive beams capable of compensating for the higher path loss at the mmWave link. Nevertheless, these benefits come at the expense of two well-known disadvantages at mmWave, which are blockage and deafness [5]–[8]. The former is due to severe attenuation induced by atmospheric absorption and penetration loss. Any obstacle in the environment may block the transmitted signal, producing significant instability in the wireless link. The latter is a consequence of using pencil-shape narrow beams, which requires an almost perfect beam alignment between the transmitter and receiver, otherwise, both ends of the link cannot see each other due to the high attenuation. Hence, both blockage and deafness will heavily complicate the initial establishment phase.

The reconfigurable intelligent surface (RIS) [9]–[14] has been intensively analysed in the field of wireless communication since it possesses great flexibility to manipulate the wireless environment and provide alternative better propagation paths between the transceivers, especially useful at mmWave to circumvent the blockage issue. Additionally, not only its fabrication cost is very competitive since it is built with low-cost passive meta-materials, but it also consumes less energy than the traditional relays since no radio-frequency chain is needed. Recently, a new generation of meta-materials has emerged. These new surfaces can perform a non-linear operation[1] that changes the frequency spectrum of the signal that was originally transmitted [15]–[17]. Let us name it as frequency shifting-RIS (FS-RIS), which is a particular case of the general RIS. Specifically, it can modify the carrier frequency of the impinging signal and reflect it in any direction of interest. Consequently, the integration of FS-RIS in the existing cellular networks has the potential to change the way we think about wireless communication.

The beam-management procedure (BMP) is a process to determine the best pair of beams between transmitter and receiver in 5G [1], especially for higher-frequency bands. The base station (BS), RIS and user equipment (UE) sequentially sweep with their respective directional beams towards different angular positions for each period [8]–[10]. Then, the UE determines the best pair of beams according to the received energy and reports this information back. On the one hand, the BMP significantly enlarges the delay of the initial access, especially when the beam width is very narrow which requires more time to cover the entire 3D space. BMP based on hierarchical beamforming can accelerate this process [8]–[10] at the expense of sacrificing the directivity and causing a range penalization, and hence those further UEs from the BS cannot be detected. On the other hand, control information may be lost due to the mentioned instability of the mmWave link, and the reliable transmission of this control information is

Kun Chen-Hu, Robin J. Williams and Petar Popovski are with the Department of Electronic Systems, Aalborg University, Denmark. E-mails: {kchenhu,rjw,petarp}@es.aau.dk. Andrea Alù is with the Advanced Science Research Center, City University of New York, and the Graduate Center, City University of New York, USA. Email: aalu@gc.cuny.edu.

The work of K. Chen-Hu, R. J. Williams and P. Popovski has been funded by the Villum Investigator Grant "WATER" from the Velux Foundation, Denmark, and the work of A. Alù has been funded by the National Science Foundation, the USA.

[1]In this paper "non-linear" refers to non-linear time invariant operation, that is, encompasses linear time-variant.

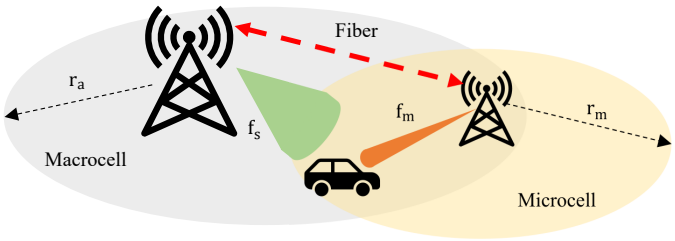

Fig. 1. Illustrative example of CoMP. Multiple BSs operated at mmWave and sub-6 GHz bands are connected by a wired link to share the information of the UEs served by each cell. The control information is spread by a macro-BS at the sub-6 GHz band, whose carrier frequency is f_s, while the mmWave link is provided by the micro-BS at f_m. The radio of each cell is given by r_a and r_m, respectively.

extremely important for synchronization and later stages. The simultaneous deployment of wireless links operated at several frequency bands at different BSs is proposed [7], also known as coordinated multi-point (CoMP) [18] (see Fig. 1). Note that CoMP is not only exploited for mmWave, but it is also relevant in sub-6 GHz bands since it can better exploit the available resources, reduce the overall interference, etc. These additional lower-frequency links correspond to those cellular networks already deployed at the existing macrocells. These networks are typically operated at the sub-6 GHz band, which possesses a larger propagation range due to their lower path-loss and a semi-directional radiation pattern capable of fully spanning each sector of the cell. These characteristics are ideal for the transportation of control information since they can be reliably spread over the entire cellular system and reach all UEs. However, this solution is complex since different BSs must be coordinated by exchanging side information related to all UEs producing an undesired overhead delay [18]. Moreover, the deployment of multiple BSs will also increase the operational cost, otherwise, standalone mmWave links could not be deployed.

To the best of our knowledge, this new non-linear capability has been tested to show its viability [15]–[17], and [19] has only analysed the theoretical bounds of this technology. However, it has never been exploited before in a wireless scenario with actual system parameters. The main scope of this work is proposing a new model for the cutting-edge FS-RIS and its integration in the particular case of mmWave cellular network for deploying communications services under mobility scenarios by exploiting the spectrum heterogeneity. The FS-RIS is capable of down-converting the carrier frequency of the signal at mmWave transmitted by the BS to a new signal whose carrier frequency belongs to the sub-6 GHz band and it is used for broadcasting the control information to the entire cell. The sub-6 GHz signal not only possesses much lower attenuation, and it can provide a more stable and reliable link and/or reach those UEs placed at the limit of the micro-cell, but it also has a broader beam width, which is capable of reducing the number of beam to sweep the entire cell, and hence decreases the executing time of the BMP. Additionally, the FS-RIS can also up-convert the signal transmitted by the UE to the mmWave BS, both for replying the control messages and sending data information. A theoretical analysis in terms of range coverage, number of available resources and overhead delay is performed for the proposed cellular networks relying on FS-RIS, and it is also compared to the existing solutions based on hierarchical BMP [8]–[10] and CoMP [7], [18], showing that the proposed architecture based on FS-RIS outperforms the techniques given in the literature. This paper is a materialization of concrete ideas for the new generation of nonlinear meta-surfaces [20].

The main contributions are summarized as follows:

- An approximated signal model for each passive element of the FS-RIS is firstly given to facilitate the description of the whole system model of a wireless system based on the FS-RIS. The resulting cascaded channel model is a generalization of the existing one [9]–[12] due to the fact that it consists of the well-known static cascaded gain produced and a new time-varying term. The former is a result of tuning the phase shifts, which can produce an alternative path between the BS and UE via FS-RIS, while the latter is a dynamic phase shift over time capable of shifting the carrier frequency of the impinged signal at each passive element.
- A mmWave cellular network relying on FS-RIS is proposed. The FS-RIS is able to down-convert the transmitted signal from the microcell BS operated at mmWave to a new signal, whose carrier frequency belongs to a sub-6GHz band in the downlink (DL), and up-convert the sub-6 GHz signal to the mmWave in the uplink (UL). Thanks to this frequency shifting, an omnidirectional/semi-directional link is obtained providing more stability and reliability. Hence, data and control information between BS↔UE via FS-RIS can be easily spread over each sector of the microcell. To show its viability, an analysis based on the link budget for the FS-RIS link is provided. This study points out that the FS-RIS can cover the same coverage area provided by the micro-BS as a consequence of facing less attenuation and noise at the receiver due to the use of lower frequency bands and narrower bandwidths, respectively.
- A novel multi-frequency BMP based on FS-RIS is proposed for carrying out the initial access procedure. Following the procedure described in 5G [1], a new BMP based on the availability of different carrier frequencies at the FS-RIS is described. The proposed technique is also hierarchical since different beam widths are jointly exploited to reduce the execution time of the procedure. Additionally, the proposed scheme does not possess the range reduction as the traditional hierarchical BMP [8]–[10], due to the exploitation of lower carrier frequencies at the FS-RIS instead of making use of fewer elements of the array to wider the beams.
- An analysis of the system performance comparison in terms of the number of available resources and the overhead delay between the proposed architecture based on FS-RIS and the existing CoMP [7], [18] is given. The performance of the proposed system outperforms the existing CoMP in terms of overhead delay since only one BS is present in the system and no information of the UEs are exchanged [7] (see Fig. 1).

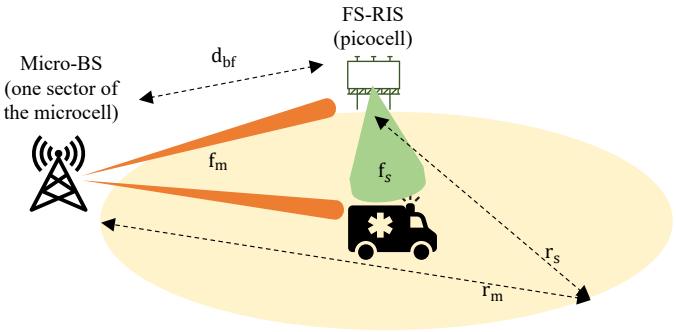

Fig. 2. Proposed mmWave scenario relying on a FS-RIS for communications under mobility scenarios. The micro-BS serves one sector of its microcell at mmWave band whose carrier frequency is f_m, while the FS-RIS can fully cover the same area of the micro-BS, which is a picocell operated at a sub-6 GHz band whose carrier frequency is f_s.

- Finally, a performance assessment based on numerical evaluation is obtained in terms of coverage range, overhead delay, maximum detectable angular speed, size of codebooks and number of available resources. All results not only verify the theoretical analysis but also highlight that the proposed architecture significantly outperforms the existing technique in the literature.

The remainder of the paper is organized as follows. Section II introduces the system model of FS-RIS-aided cellular network. Section III details the proposed approximated signal model of the FS-RIS is explained. Section IV analyses the range of an FS-RIS link and the parameters to be configured to have the same coverage range as the micro-BS. Section V proposes the multi-frequency BMP for a mmWave cellular system relying on FS-RIS. Section VI analyses the system performance of a FS-RIS assisted network in terms of the number of available resources and the overhead delay. Section VII presents several numerical results for the proposed architecture, providing an assessment of the achieved performance. Finally, in Section VIII, the conclusions are disclosed.

II. System Model

The entities involved in the considered scenario are summarized in Fig. 2. One micro-BS is serving a particular sector of a microcell operated at mmWave, whose carrier frequency and bandwidth are denoted by f_m and B_m, respectively. In terms of the size of the coverage area, the microcell is (partially) covering a specific area within a macrocell. According to [21], the radio of the macrocell and microcell are $r_a = 500$ m and $r_m = 200$ m, respectively. A UE of interest is being served, which is not only operated at the mmWave, but it also works at sub-6 GHz, whose carrier frequency and bandwidth are denoted by f_s and B_s, respectively. Finally, one FS-RIS is also deployed within the sector of the microcell, which is capable of shifting the carrier frequency of the impinging signal, either down or up ($f_m \leftrightarrow f_s$). In order to ease the notation and for the sake of space, only one FS-RIS is considered in the description of the novel multi-frequency BMP. Later, the operation with multiple FS-RISs is assumed to analyse the number of available resources and the delay overhead.

The micro-BS is equipped by a uniform planar array (UPA), whose number of elements is given by $M_B = M_B^x M_B^y$, where M_B^x and M_B^y are the number of elements in the x and y-axis, respectively. The horizontal and vertical distance between each two contiguous elements are both separated by d_B^x and d_B^y, respectively. Assuming that $d_B^x = d_B^y = \frac{\lambda_m}{2}$, the response of steering vector at the antenna element (b_x, b_y) is given by

$$a_B\left(\phi_B, \theta_B, \lambda_m, b_x, b_y\right) = \exp\left(j\frac{2\pi}{\lambda_m}\xi_B\right), \quad \lambda_m = f_m/c, \quad (1)$$

$$\xi_B = \frac{\lambda_m}{2}\left(b_x \sin\left(\theta_B\right)\cos\left(\phi_B\right) + b_y \sin\left(\theta_B\right)\sin\left(\phi_B\right)\right), \quad (2)$$

where $0 \le b_x < M_B^x$, $0 \le b_y < M_B^y$, λ_m is the wavelength of the signal, c denotes the speed of the light, ξ_B corresponds to the phase array factor produced by the UPA and the azimuth and elevation angles are given by ϕ_B and θ_B, respectively. Analogously to the BS, the FS-RIS is also equipped with a UPA of frequency shifter passive and reflecting elements. The number of the passive elements is given by $M_F = M_F^x M_F^y$, and the separation distance between contiguous passive elements are also $d_F^x = d_F^y = \frac{\lambda_m}{2}$. The expression of its steering vector is the same as (1)-(2), by replacing the subindex B by F. On the contrary, the UE is only equipped with one single antenna. Moreover, it is assumed that all radiating elements from the BS, FS-RIS and UE have an omnidirectional diagram pattern.

The distance between the BS↔FS-RIS, BS↔UE and FS-RIS↔UE are given by d_{bf}, d_{bu} and d_{fu}, respectively, measured in meters. The channel impulse responses between the BS↔FS-RIS and BS↔UE can be described as a single tap line-of-sigh (LOS) model. This assumption is a consequence of the presence of extremely high path-loss induced by the mmWave, and hence the pencil-sharp beams will only point towards the strongest LOS path. Hence, these channel responses can be expressed as [22]

$$h_{bu}\left[\tau\right] = \frac{1}{\sqrt{l_{bu}}}\delta\left[\tau - \tau_{bu}\right], \quad h_{bf}\left[\tau\right] = \frac{1}{\sqrt{l_{bf}}}\delta\left[\tau - \tau_{bf}\right], \quad (3)$$

where l_{bu} and l_{bf} are the path-loss between BS↔UE and BS↔FS-RIS, respectively, and τ_{bu} and τ_{bf} denote the delay of the link between BS↔UE and BS↔FS-RIS, respectively. On the other hand, the channel between the FS-RIS↔UE is described by a multi-path channel, where it may possess a LOS path while others are non-LOS (NLOS) ones since the carrier frequency of the channel belongs to the sub-6 GHz, and its expression is given by

$$h_{fu}\left[\tau\right] = \frac{1}{\sqrt{l_{fu}}}\sum_{i=1}^{N_{fu}}\alpha_{fu,i}\delta\left[\tau - \tau_{fu,i}\right], \quad (4)$$

where l_{fu} is the path-loss of the link between FS-RIS↔UE, N_{fu} corresponds to the number of taps between the channel of FS-RIS↔UE, $\alpha_{fu,i}$ and $\tau_{bu,i}$ denote the small-factor channel coefficient and the delay of the i-th tap, respectively.

To show the feasibility of the proposed architecture in a realistic system, the chosen signal model corresponds to the well-known orthogonal frequency division multiplexing (OFDM). Following the 5G [1], the frame period value (T_{frame}) is constrained by the standard, and then, a multi-numerology OFDM

signal is adopted within this frame period. The numerology of the mmWave and sub-6 GHz sub-networks are labelled by the integer numbers μ_m and $\mu_s \in \{0, \ldots, 3\}$, respectively, which will determine their corresponding parameters of the OFDM signal, such as number of subcarriers, subcarrier spacing, OFDM symbol and sample duration, etc. More details are given in Section VI.

III. Proposed Approximated FS-RIS Signal Model

To show the potential benefits of the FS-RIS in a realistic communication scenario and facilitate the description of the whole system, an approximated model is introduced for each passive element of the FS-RIS, which can be modelled as a cascade connection of a dual bandpass filter, an attenuator and a time-varying termination. The first element is responsible for limiting the bandwidth of the impinged and reflected signals, the second one only reduces the power strength of the impinged signal, while the latter reflects the impinged signal modulated at a different carrier frequency. Each element is detailed in the following subsections.

A. Time-Varying Termination and Attenuation

The reflection coefficient of each passive element of the FS-RIS is modelled in discrete time, where n represents the discrete time index and the sampling period is T. To obtain an accurate enough model, the sampling period should satisfy the Nyquist sampling theorem ($T \leq T_m/2$), where $T_m = (f_m + B_m/2)^{-1}$. Hence, the expression of the reflection coefficient is given as

$$\Gamma_{f_x,f_y}[n] = \frac{1}{\sqrt{l_F}} \exp\left(j\psi_{f_x,f_y}\right) \exp\left(j\psi_n\right), \tag{5}$$

where $0 \leq f_x < M_F^x$, $0 \leq f_y < M_F^y$, l_F is the total attenuation produced by the passive element, such as coupling effects, parasite losses, etc. ψ_{f_x,f_y} denotes the traditional static phase shift of each passive element, responsible for performing the beamforming (spatial modulation) and can be designed according to [9]–[12], while ψ_n is the dynamic phase shift, in charge of providing the carrier frequency shift (temporal modulation), and all passive elements of the meta-surface share the same dynamic phase shift. To either down or up-convert the carrier frequency of the impinging signal, the dynamic phase shift must provide a constant variation of the phase, such that $\psi_n = \pm 2\pi f_F n$, where f_F is the mixing frequency at the FS-RIS. The time-varying termination plays the role of a traditional mixer-based frequency converter. Note that the FS-RIS is fully backward compatible to the regular RIS, either passive [9]–[12] or active [14], since the static phase shift can be obtained by exploiting existing solutions in the literature.

B. Dual Bandpass Filter

Since the FS-RIS can change the carrier frequency of the impinged signal ($f_m \leftrightarrow f_s$), the passband filter must have, at least, two passbands centred at these two carrier frequencies, f_m at mmWave and f_s at sub-6 GHz. The width of the band-pass at sub-6 GHz is denoted by B'_s, which must be wider than

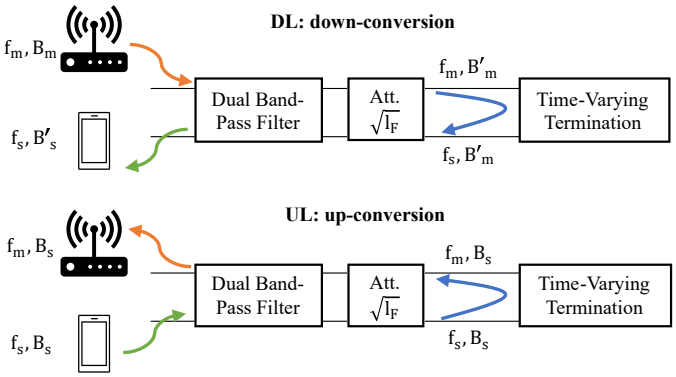

Fig. 3. Approximated model of carrier frequency shifting operation by each passive element of the FS-RIS at DL (top) and UL (bottom).

or equal to the bandwidth of the sub-6 GHz signal ($B_s \leq B'_s$) to avoid any information loss. The width of the passband at mmWave band is denoted by B'_m, which may be narrower than the bandwidth of the mmWave signal transmitted by the BS, however it must be wider than or equal to the bandwidth of the passband at sub-6 GHz ($B_m \geq B'_m \geq B'_s$), ensuring that the information carried by sub-6 GHz signal remains untouched. In Fig. 3, an example of the frequency shifting for both DL and UL is depicted. In DL, the impinging signal is firstly filtered ($B_m \rightarrow B'_m$), then the reflecting element is down-converting the signal ($f_m \rightarrow f_s$). Finally, the dual bandpass filter only keeps those part of the signal that corresponds to the sub-6 GHz ($B'_m \rightarrow B'_s$). In the UL, an up-conversion is performed at the reflecting element, and the bandwidth of the signal is ideally not changed since the bandwidth of the impinged signal is smaller than the bandwidth of the passbands ($B_s \leq B'_s \leq B'_m$). For the sake of conciseness and ease of the notation, it is assumed that this dual band pass filter is a loss-less element, and its multi-tap effect is already included in the multi-path channel between the FS-RIS↔UE given in (4), similar to the bandpass filters placed at the transmitter and receiver.

C. The Cascaded Channel Model

Without loss of generality and for the sake of space, only the DL case is considered in this paper, while the UL case can be analogously obtained. The gains produced by the UPA at the BS and FS-RIS are

$$g_B(\phi_B, \theta_B) = \sum_{b_x=1}^{M_B^x} \sum_{b_y=1}^{M_B^y} a_B\left(\phi_B, \theta_B, \lambda_m, b_x, b_y\right) \tag{6}$$

$$\begin{aligned} g'_F\left(\phi_F^m, \theta_F^m, \phi_F^s, \theta_F^s, n\right) &= \sum_{f_x=1}^{M_F^x} \sum_{f_y=1}^{M_F^y} \Gamma_{f_x,f_y}[n] \\ &\times a_F\left(\phi_F^m, \theta_F^m, \lambda_m, f_x, f_y\right) a_F\left(\phi_F^s, \theta_F^s, \lambda_s, f_x, f_y\right), \end{aligned} \tag{7}$$

respectively, where λ_m and λ_s are the wavelength of impinged (mmWave) and reflected (sub-6 GHz) signals, respectively. The angles with super-index m denote the angles of arrival at mmWave, while the angles with super-index s account for the departure angles at sub-6 GHz.

By substituting (5) in (7), it can be simplified as

$$g'_F\left(\phi_F^m,\theta_F^m,\phi_F^s,\theta_F^s,n\right)=\frac{\exp\left(\pm j2\pi f_F n\right)}{\sqrt{l_F}}\times g_F\left(\phi_F^m,\theta_F^m,\phi_F^s,\theta_F^s,\psi_{f_x,f_y}\right), \tag{8}$$

where $g_F\left(\phi_F^m,\theta_F^m,\phi_F^s,\theta_F^s,\psi_{f_x,f_y}\right)$ corresponds to the static gain produced by the meta-surface and $\exp\left(\pm j2\pi f_F n\right)$ denotes the dynamic phase modulation performed at the meta-surface.

The cascaded channel between the BS and UE via FS-RIS is given by

$$\begin{aligned}h_{bfu}\left[n,\tau\right]&=\frac{1}{\sqrt{l_{bf}l_{fu}l_F}}g_B\left(\phi_B,\theta_B\right)\\&\times\sum_{i=0}^{N_{fu}}\alpha_{fu,i}g_F\left(\phi_{F,i}^m,\theta_{F,i}^m,\phi_{F,i}^s,\theta_{F,i}^s,\psi_{f_x,f_y}\right)\\&\times\exp\left(\pm j2\pi f_F\left[n-\tau_{bf}-\tau_{fu,i}\right]\right)\delta\left[\tau-\tau_{bf}-\tau_{fu,i}\right],\end{aligned} \tag{9}$$

According to [9]–[12], the static phase configuration given in $g_F\left(\phi_{F,i}^m,\theta_{F,i}^m,\phi_{F,i}^s,\theta_{F,i}^s,\psi_{f_x,f_y}\right)$ is designed to maximize the gain of the cascaded channel, which consists on choosing that phase configuration capable of jointly selecting the best taps of the BS↔FS-RIS and FS-RIS↔UE channels. Meanwhile, the time-varying reflection shifts the carrier frequency of the impinged wave by the mixing frequency f_F. This proposal is very flexible since a greater variety of amount resulting carrier frequencies can be obtained, unlike as compared to [16], where only a subset of harmonic frequencies are available by using a set of predetermined values for time-varying phase configuration at the RIS (ψ_n). Moreover, note that the cascaded channel also points out that this alternative link is also suffering from a double path-loss effect, which can be also compensated by using active RIS [14].

IV. Analysis of the Coverage Range of a mmWave Cellular Network assisted by an FS-RIS.

In this section, the analysis of the coverage range of a mmWave cellular network assisted by the novel FS-RIS based on the computation of the link budgets between the micro-BS and UE (direct path and reflected path via FS-RIS) is given. The main aim of this analysis is to showcase that the coverage provided by the micro-BS operated at the mmWave (one sector of the microcell) and the FS-RIS operated at the sub-6 GHz (picocell) have the same range, and hence both sub-networks can serve all the UEs placed in the same area of interest, unlike the coverage mismatch produced by the case of CoMP [7].

In Fig. 4, the timing diagram of the proposed multi-frequency BMP for a mmWave cellular network assisted by an FS-RIS is shown, where $N_{\text{symb,m}}^{\text{frame}}$ is the number of OFDM symbols within one frame for the mmWave signal. The FS-RIS is down-converting the mmWave signal operated at f_m to a sub-6 GHz operated at f_s. Since the latter has a wider beam width and lower path loss, it is useful to perform an initial fast beam-sweeping through the area of interest. According to 5G standard [1], the micro-BS is spreading the synchronization signal block (SSB) through all directions. Then, the UE will choose the best beam and report it back to the micro-BS in the next beam-sweeping period. Given the information of the best beam of a UE of interest at f_s, the micro-BS will perform a second beam-sweeping at the mmWave band (f_m), focusing only in that area covered by the previously chosen beam at f_s, instead of sweeping the whole 3D space, and hence the latency is significantly reduced. Finally, the UE is reporting again the newly chosen mmWave beam by using the already established communication via sub-6 GHz band (f_s), which keeps reducing the latency of the system.

A. Link-Budget of the Direct Link at mmWave

The link budget of the direct path between BS↔UE operated at the mmWave is firstly computed as a reference case since it will establish the radius of the microcell. The received power of a UE of interest operated at f_m is given by

$$P_{r,m}\left[\text{dBm}\right]=P_t\left[\text{dBm}\right]+G_B-L_{bu}-10\log_{10}\left(N_B\right), \tag{10}$$

$$G_B\left[dB\right]=10\log_{10}\left(g_B\right),\quad L_{bu}\left[dB\right]=10\log_{10}\left(l_{bu}\right), \tag{11}$$

where P_t is averaged transmitted power at the micro-BS per subcarrier, $P_{r,m}$ denotes the average received power at the UE in the mmWave per subcarrier, G_B corresponds to the gain provided by the antenna array at the BS in dB, L_{bu} accounts for the path-loss between the BS↔UE in dB and N_B represents the number of simultaneous beams established by the micro-BS. The path-loss is modelled by log-distance model [22], which is described as

$$L_{bu}\left[\text{dB}\right]=L_0\left(f_m,r_0\right)+10\gamma\log_{10}\left(\frac{r_m}{r_0}\right), \tag{12}$$

$$L_0\left(f_m,r_0\right)\left[\text{dB}\right]=20\log_{10}\left(\frac{4\pi}{c}\right)+20\log_{10}\left(f_m\right)+20\log_{10}\left(r_0\right), \tag{13}$$

where r_0 is the reference distance and γ corresponds to the path-loss exponent.

Taking into account (10)-(13), the maximum radius of the microcell can be computed by making use of the minimum required received power by the receiver $P_{r,m}=P_{r,m}^{\min}$. Assuming that the receiver is only limited by the AWGN, this minimum power can be defined as

$$P_{r,m}^{\min}\left[\text{dBm}\right]\geq 10\log_{10}\left(B_m\right)+S_n\left[\text{dBm/Hz}\right], \tag{14}$$

where S_n is the noise power spectral density.

Substituting (14) in (10), the maximum radius of the microcell is given by

$$10\gamma\log_{10}\left(\frac{r_m^{\max}}{r_0}\right)=P_t-P_{r,m}^{\min}+G_B-L_0\left(f_m,r_0\right)-10\log_{10}\left(N_B\right). \tag{15}$$

Inspecting (15), the range of the microcell mainly depends on the chosen carrier frequency (attenuation) and used bandwidth (minimum received power) for a given transmit power and antenna array.

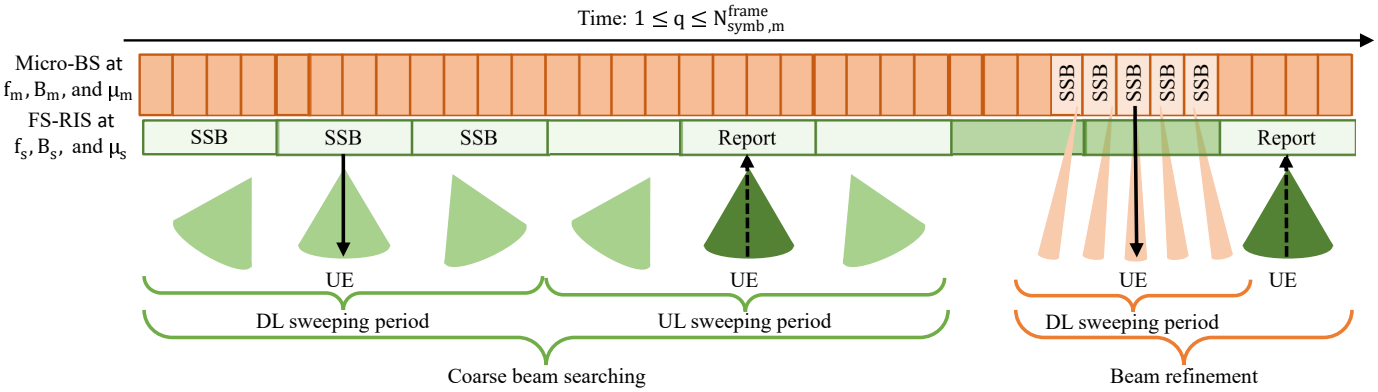

Fig. 4. Time diagram of the proposed multi-frequency BMP in mmWave system relying on FS-RIS. The sub-6 GHz signal obtained from FS-RIS can provide wider beams and perform a fast initial beam-sweeping, meanwhile, the micro-BS is using the narrow directive beams at the mmWave to refine the position of the UE. The second beam-sweeping at mmWave is only performed in that area that matches the previously chosen beam at sub-6 GHz, and the beam report is also reported back via the chosen sub-6 GHz beam.

B. Link-Budget of the Reflected Link via FS-RIS at Sub-6 GHz

Then, the link budget of the reflected link (BS↔FS-RIS↔UE) operated at a lower carrier frequency is also given. The received power of the UE of interest operated at f_s is given by

$$P_{r,s}\,[\text{dBm}] = P_t\,[\text{dBm}] + G_B + G_F - 10\log_{10}(N_B) - L_{bf} - L_F - L_{fu}, \tag{16}$$

$$G_F\,[dB] = 10\log_{10}(g_F), \quad L_F\,[dB] = 10\log_{10}(l_F), \tag{17}$$

$$L_{bf}\,[dB] = 10\log_{10}(l_{bf}), \quad L_{fu}\,[dB] = 10\log_{10}(l_{fu}), \tag{18}$$

where G_F is the gain provided by the array at the FS-RIS in dB, while L_{bf} and L_{fu} correspond to the path-loss between BS↔FS-RIS and FS-RIS↔UE in dB, respectively, and L_F is the loss induced by each passive element of the FS-RIS in dB.

Again, the minimum received power in the UE at f_s can be computed by using (14) by replacing the value of the bandwidth by B_s. Therefore, the maximum radius is given by

$$10\gamma\log_{10}\left(\frac{r_s^{\max}}{r_0}\right) = P_t - P_{r,s}^{\min} + G_B + G_F - 10\log_{10}(N_B) - L_0(f_m, d_{bf}) - L_F - L_0(f_s, r_0). \tag{19}$$

According to the range requirement imposed at the beginning of this section, the range of the FS-RIS should be equal to or larger than the range of the microcell ($r_m \leq r_s$) to ensure that both sub-networks can serve the same UEs placed in the area of interest. Consequently, one sector of the microcell operated at the mmWave will geographically correspond to a picocell operated at the sub-6 GHz via FS-RIS, see Fig. 2. By comparing (15) and (19), it can be obtained that

$$10\log_{10}\left(\frac{B_m}{B_s}\right) + G_F + 20\log_{10}\left(\frac{c}{4\pi}\right) \geq 20\log_{10}(f_s) + 20\log_{10}(d_{bf}) + L_F. \tag{20}$$

By inspecting (20), it states how to choose the different parameters to increase the range of the picocell driven by the FS-RIS and provide the same coverage area of one sector of the microcell. To satisfy the inequality imposed by (20), its left part should be increased meanwhile its right part should be reduced. On the one hand, to increase the left part of (20), a higher gain of the FS-RIS at the cascaded link (G_F) is required, since it will significantly amplify the power of the reflected signal. This gain can be enhanced by increasing the number of used passive elements at the FS-RIS (M_F). Moreover, the bandwidth of the reflected signal by the FS-RIS should be much lower than the bandwidth of the original mmWave signal ($B_m >> B_s$). A reduced bandwidth will decrease the total noise at the receiver, and hence the range is enlarged. This requirement can be easily satisfied since the reflected signal belongs to a sub-6 GHz signal, and its bandwidth is always proportional to its carrier frequency due to the constraints of hardware implementation. On the other hand, to reduce the right part of (20), the carrier frequency of the reflected signal by the FS-RIS (f_s) should be as low as possible. Hence, a down conversion is preferred since its corresponding path loss is also lower. The additional attenuation produced by each passive element of the FS-RIS (L_F) is also relevant to increasing the range of the picocell and it should be as low as possible, otherwise, the whole system collapses. Finally, the distance between the micro-BS and deployed the FS-RIS (d_{bf}) should be also shortened to decrease its corresponding path loss.

All these parameters should be jointly considered to shape the coverage area of the picocell within any sector of the microcell. Typically, the carrier frequencies and bandwidths (f_m, f_s, B_m and B_s) are imposed by the standard and the chosen numerology of the signal, such as 5G [1]. The attenuation and gain (L_F and G_F) of the FS-RIS are characterized by the used hardware components and their corresponding imperfections, specifically the entire system is seriously compromised if L_F is excessively high. The distance between the BS ↔ FS-RIS (d_{bf}) is limited by the geographical restrictions, which are imposed where the FS-RIS can be physically deployed. Moreover, the result given in (20) showed that the proposed system is very flexible in terms of configuration and deployment of FS-RIS in the existing cellular networks since the coverage

area provided by the FS-RIS can be easily shaped according to geographical restrictions, hardware limitations and chosen numerologies.

V. Novel Multi-Frequency BMP in mmWave Cellular Networks assisted by FS-RIS

The BMP is extremely relevant in mmWave communication systems due to the issues related to blockage and deafness [7], as mentioned before. In this section, the full procedure of the novel multi-frequency BMP for the proposed FS-RIS-assisted mmWave cellular network described, in Fig. 4, is detailed. Since there are two sub-networks (one sector of the microcell operated at mmWave band and another picocell operated at sub-6 GHz band thanks to the FS-RIS), the proposed procedure is progressive since any UE must first attach to the micro-BS through the FS-RIS operated at a lower carrier frequency (f_s), and then the UE will be allowed to directly attach to the mmWave network (f_m). During this two-step procedure, the accuracy of the angular position of each UE is also progressively improved at each stage with a reduced beam-sweeping time. This fact comes as a consequence of using a different beam width at each stage due to the exploitation of multiple carrier frequencies (f_m and f_s) and the availability of a coarse angular estimation given by the previous stage, and therefore the BMP only has to sweep a specific area out of the whole 3D space.

Comparing the proposed technique to the existing ones in the literature. On the one hand, the proposed architecture also follows the concept of hierarchical BMP [8]–[10] by using beams of several widths. However, the range of the picocell via FS-RIS is not reduced since the wider beams exploited in the BMP are a consequence of using lower carrier frequencies obtained at the FS-RIS, instead of deactivating antennas elements in the hierarchical BMP [8]–[10]. On the other hand, the proposed technique is similar to the CoMP [7] due to the fact that multiple carrier frequencies are jointly exploited in the BMP. However, the overhead delay induced by the control information exchange among multiple BSs is avoided [18], since only one micro-BS is presented in the proposed architecture. The proposed BMP based on FS-RIS is detailed in the following subsections by making use of the protocols of 5G [1], where multiple UEs can be considered. Furthermore, the proposed technique can be also integrated into other communication standards.

A. Coarse Beam Searching via FS-RIS at Sub-6 GHz (f_s)

The main objective of making use of a sub-6 GHz signal is to spread the control information of the micro-BS throughout the whole sector of the microcell and find out the maximum number of UE interested in entering the system within the shortest possible period (see the left part of Fig. 4). The mmWave micro-BS firstly broadcasts the control information by using the SSB through the FS-RIS operated at the lower carrier frequency and bandwidth ($f_s << f_m$ and $B_s << B_m$). This choice has mainly three advantages, a reduced path loss (replacing f_m by f_s in (13)), a lower noise at the receiver (replacing B_m by B_s in (14)) and an increased beam width (replacing f_m by f_s in (1)-(2)). The former two aspects will provide a more reliable and stable link by avoiding the blockage and deafness issues existing at the mmWave. The latter will reduce the number of required beams to sweep the whole sector of the microcell, therefore reducing the latency of the system. Then, all UEs can measure their received energy and report back to the micro-BS the chosen beam in the next sweeping period via FS-RIS. At the end of this stage, a coarse estimation of the angular position of all UEs may be computed, which will be improved in the following stage. According to Fig. 4, the green beams operated at f_s are much wider than the orange one operated at f_m. The SSB is spread by the beam-sweeping making use of wider beams operated at f_s, then the UE will report the best beam in the next beam-sweeping period.

Note that even though the beam width is widened at the FS-RIS and its corresponding gain is lowered ($G_F(f_s) \downarrow$), the coverage range of the FS-RIS is still capable of covering the entire sector of the microcell ($r_m \leq r_s$), thanks to the reduction path-loss between the FS-RIS and UE ($L_{fu} \downarrow$) and the noise reduction provided by the down-conversion of the carrier frequency and bandwidth reduction ($f_s << f_m$ and $B_s << B_m$). However, this stage is not able to provide accurate enough angular positions of any UE due to the use of these wide beams, and consequently, it must be refined by the following stages.

The codebook C_s at the FS-RIS is built by N_s codewords as follows

$$C_s \in \left\{\mathbf{c}_{s,0}, \ldots, \mathbf{c}_{d,N_s}\right\}, \quad \mathbf{c}_{s,i} \leftrightarrow \left(\phi_{s,i}, \Delta\phi_{s,i}, \theta_{s,i}, \Delta\theta_{s,i}\right), \tag{21}$$

where $\mathbf{c}_{s,i}$ is the i-th codeword vector of M_F elements and it can cover a specific plane, $\phi_{s,i}$ and $\Delta\phi_{s,i}$ are the initial angle and angle length in azimuth, respectively, while $\theta_{s,i}$ and $\Delta\theta_{s,i}$ are the initial angle and angle length in elevation, respectively. Considering (7)-(9), each codeword for the static phase configuration can be obtained as

$$\begin{aligned} \mathbf{c}_{s,i} = {} & \angle\left(a_F^*\left(\phi_F^m, \theta_F^m, \lambda_m, f_x, f_y\right)\right) \\ & + \angle\left(a_F\left(\phi_{s,i} + \frac{\Delta\phi_{s,i}}{2}, \theta_{s,i} + \frac{\Delta\phi_{s,i}}{2}, \lambda_s, f_x, f_y\right)\right), \\ i = {} & M_x\left(f_x - 1\right) + f_y, \quad 0 \leq f_x < M_F^x, \quad 0 \leq f_y < M_F^y, \end{aligned} \tag{22}$$

where $\angle(\cdot)$ is obtaining the phase of the argument. The first two terms are matching the channel between BS↔FS-RIS, while the last one is responsible for sweeping the whole space. Note that the dynamic phase shift is assumed to be provided by the time-varying termination after setting the value of f_F (see Fig. 3). Otherwise, the additional term $\psi_n = \pm 2\pi f_F n$ must be added to the expression given in (22).

During this procedure, the micro-BS will find out the best beam at the FS-RIS capable of serving each UE ($\mathbf{c}_{s,i^*}$) and the plane given by $\left(\phi_{s,i^*}, \Delta\phi_{s,i^*}, \theta_{s,i^*}, \Delta\theta_{s,i^*}\right)$ that contains the coarse angular position of each UE. The latency of this process is not excessively large since the beam width is semi-directional. Moreover, this initial coarse estimation will also alleviate the execution time of BMP in the following stage operated at mmWave.

B. Beam Refinement at mmWave micro-BS (f_m)

Once the UE is attached to the micro-BS via FS-RIS and a stable connection is kept in the picocell at f_s via FS-RIS, the UE may enter the mmWave sub-network. The main objective of this system is to provide the desired ultra-wideband link operated at mmWave. Again, the BMP is executed to find out the best pencil-shape narrow beam to serve a UE of interest (see the right part of Fig. 4). However, instead of sweeping the whole sector of the microcell, the micro-BS will make use of the knowledge obtained by the previous stage and only sweep those directions provided by the coarse estimation of the angle positions of all UEs. In Fig. 4, the orange narrow beams operated at f_m from micro-BS are only sweeping a small space out of the whole 3D space, and hence the executing time of the BMP is significantly reduced. Again the SSB is spread by the beam-sweeping, however, the report is immediately sent by the UE to the micro-BS through the sub-6 GHz sub-network via FS-RIS, and hence the execution time of the BMP is also reduced by using the FS-RIS. Note that, the exploitation of narrow directive beams at mmWave could also assist in those services based on target localization.

Analogously to the FS-RIS, the codebook C_m at the BS is built by N_m codewords as follows

$$C_m \in \left\{\mathbf{c}_{m,0}, \ldots, \mathbf{c}_{m,N_m}\right\}, \quad \mathbf{c}_{m,i} \leftrightarrow \left(\phi_{m,i}, \Delta\phi_{m,i}, \theta_{m,i}, \Delta\theta_{m,i}\right). \tag{23}$$

Due to the use of pencil-shape narrow beams at mmWave, and by comparing (21) and (23), it should satisfy that

$$N_s << N_m, \quad \Delta\phi_{s,i} >> \Delta\phi_{m,i}, \quad \Delta\theta_{s,i} >> \Delta\theta_{m,i}, \tag{24}$$

where the number of codewords at the mmWave should be much larger than the previous one since the area covered by each codeword is significantly smaller. The expression for each codebook is the same as given in (22) by replacing the sub-index s by m.

By making use of the condition given in (24) and the availability of the chosen codeword in the previous sub-network ($\mathbf{c}_{s,i^*}$), the latency induced by the BMP at mmWave can be significantly reduced since only a subset of codewords ($C'_m \subset C_m$) is used to retrieve accurate enough angular position of each UE, which satisfy that

$$\begin{aligned} C'_m \in \big\{\mathbf{c}_{m,j} \mid \; & \phi_{s,i^*} \le \phi_{m,j} + \Delta\phi_{m,j} \le \phi_{s,i^*} + \Delta\phi_{s,i^*}, \\ & \theta_{s,i^*} \le \theta_{m,j} + \Delta\theta_{m,j} \le \theta_{s,i^*} + \Delta\theta_{s,i^*}\big\}. \end{aligned} \tag{25}$$

Consequently, C'_m is a reduced codebook built by N'_m codewords, which corresponds to only those codewords of the mmWave link that sweep the 3D space constrained by the chosen codeword at the previous stage operated at sub-6 GHz band. Therefore, it satisfies that

$$N_c = N_s + N'_m << N_m, \tag{26}$$

where N_c is the total number of used codewords, and it points out that the BMP based on the combination of the two codebooks C_s and C'_m operated at f_s and f_m, respectively, is significantly faster than sweeping the whole 3D space by using C_m. Note that to keep reducing the executing time of the whole BMP ($N_C \downarrow$), several FS-RISs can be simultaneously exploited and operated at different carrier frequencies and beam widths, as shown in Section VII.

VI. Analysis of the System Performance in FS-RIS Assisted Networks

A theoretical analysis of the system performance in terms of the number of available resources for data transmission and the overhead delay for the proposed architecture based on FS-RIS is given, and it is also compared to the existing CoMP case [7], [18]. The overall performance depends on the chosen resource allocation strategy adopted at the micro-BS [23]–[27]. Since the development of the scheduler is out of the scope of this work, a multi-numerology resource allocation algorithm based on dealing with each sub-network as an independent system from others is assumed [27]. Two cases of sub-network resource allocation are presented, denoted as parallel and sequential operation modes, to allow the theoretical evaluation of the number of available resources and the overhead delay of the proposed system. The results will show that the proposed system outperforms the existing CoMP in terms of overhead delay since only one micro-BS is present in the system and no information of the UEs are exchanged [7] (see Fig. 1). Moreover, some modifications performed at the operation modes can keep reducing the executing time of the BMP by allowing the transmission of the beam report via the previously established sub-6 GHz link via FS-RIS, and at the same time, avoiding a significant degradation of the number of available resources. Consequently, the proposed system is more appealing for high-capacity communications under mobility scenarios, since the system is able to get accurate channel estimates of each UE more frequently.

A. Resource Allocation at a Multi-Numerology System

Following the 5G standard [1], the number of OFDM symbols per frame and the OFDM symbol period is given by

$$N^{\text{frame}}_{\text{symb},e} = 2^{\mu_e} N^{\text{slot}}_{\text{symb}} N^{\text{frame}}_{\text{slot}}, \quad T_{\text{symb},e} = \frac{T_{\text{frame}}}{N^{\text{frame}}_{\text{symb},e}}, \quad e \in \{m, s\}, \tag{27}$$

where the subindex e is a token, $N^{\text{slot}}_{\text{symb}}$ is the number of OFDM symbols per slot and $N^{\text{frame}}_{\text{slot}}$ denotes the number of slots per frame. The number of subcarriers per OFDM symbol and its corresponding bandwidth are given by

$$N^{\text{symb}}_{\text{sc},e} = N^{\text{RB}}_{\text{sc}} N^{\text{symb}}_{\text{RB},e}, \quad B_e = 2^{\mu_e} \Delta f N^{\text{symb}}_{\text{sc},e}, \quad e \in \{m, s\}, \tag{28}$$

where $N^{\text{RB}}_{\text{sc}}$ accounts for the number of subcarriers per resource block (RB) and $N^{\text{symb}}_{\text{RB},m}$ denotes the number of RB per OFDM symbol and Δf is the subcarrier spacing measured in Hertz.

According to (27) and (28), the resource grid defined by the set $\mathcal{R}$ of is given by

$$\mathcal{R} = \left\{(k, q), \;\; k = 1, \ldots, \frac{B_m}{\Delta f}, \;\; q = 1, \ldots, N^{\text{frame}}_{\text{symb},m}\right\}, \tag{29}$$

where k and q are the frequency and time resource indices. Typically, the resource grid is defined by the mmWave numerology since it has the largest bandwidth (total amount of frequency bins) and the smallest sampling time for a given frame duration (total amount of time bins).

Due to the heterogeneous scenario where several sub-networks are operated at different numerologies [25]–[27], the minimum resource unit to be allocated depends on the parameters of each sub-network, defined as follows

$$\begin{aligned}\mathcal{R}_{\min,e}\left(k_e,q_e\right)=\{\ (k,q)\,,\quad & k_e 2^{\mu_e}<k\leq\left(k_e+1\right)2^{\mu_e},\\ & q_e 2^{\mu_{\max}-\mu_e}<q\leq\left(q_e+1\right)2^{\mu_{\max}-\mu_e}\ \}\,,\quad e\in\{m,s\}\,,\end{aligned} \tag{30}$$

where k_e and q_e are the resource indexes at the e-th sub-network. Consequently, the scheduler will allocate the available resources to each sub-network according to (27)-(30), and they must also satisfy that $\mathcal{R}_m,\mathcal{R}_s\subset\mathcal{R}$ and $\mathcal{R}_s\cup\mathcal{R}_m=\emptyset$, where $\mathcal{R}_m$ and $\mathcal{R}_s$ are the set of allocated resources for the mmWave and sub-6 GHz sub-networks, respectively. Then, the total achievable rate of the system corresponds to the sum of all sub-networks as follows

$$R\,[\text{bps/Hz}]=\sum_{e\in\{m,s\}}\frac{\left|\mathcal{R}_{\min,e}\right|}{|\mathcal{R}|}\sum_{(k,q)\in\mathcal{R}_e}\log_2\left(1+p_t^{k,q}\frac{\left|\tilde{h}_e^{k,q}\right|^2}{\sigma_e^2}\right), \tag{31}$$

$$\tilde{h}_e^{k,q}\in\left\{\tilde{h}_m^{k,q},\tilde{h}_s^{k,q}\right\},\quad \sigma_e^2=B_eS_n,\quad P_t=10\log_{10}\left(\mathbb{E}\left\{p_t^{k,q}\right\}\right), \tag{32}$$

where $p_t^{k,q}$ is the allocated power at (k,q)-th resource in Watts, $\mathbb{E}\{\bullet\}$ is the expectation operation performed in the frequency and time resource indexes, $\tilde{h}_e^{k,q}$ denotes the channel frequency response for the e-th sub-network at (k,q)-th resource, $\tilde{h}_m^{k,q}$ and $\tilde{h}_s^{k,q}$ are the channel frequency response for the direct ($h_{bu}\,[\tau]$) and reflecting ($h_{bfu}\,[t,\tau]$) paths, respectively at (k,q)-th resource.

The rate maximization problem constrained by the available power can be described as

$$\begin{aligned}&\max_{p_e^{k,q},\mathcal{R}_m,\mathcal{R}_s}\quad R\\ &\text{s.t.}\ \sum_e\sum_{(k,q)\in\mathcal{R}_e}p_e^{k,q}\leq P_{\max}\,[\text{Watts}]\,,\quad R\geq R_{q,e},\quad e\in\{m,s\}\,,\end{aligned} \tag{33}$$

where $R_{q,e}$ is the minimum requested rate by the higher layers at the e-th sub-network. Eq. (33) is a resource allocation problem capable of dealing with multiple sub-networks operated at different numerologies which are sharing the same resource grid [25]–[27]. The simultaneous operation of several sub-networks with different numerologies is a consequence of using a mmWave radio-frequency chain equipped at the micro-BS and all the reflected signals from the FS-RISs are down-converted to the sub-6 GHz band.

The resolution of the resource allocation problem is out of the scope of this work, however, the complexity induced by solving a real-time non-convex optimization will negatively impact in the overall system. Therefore, a numerology-oriented resource allocation strategy is assumed to alleviate the computational complexity of solving the joint resource allocation problem and allow the analysis of the performance of the proposed architecture in terms of the number of available resources and overhead delay. The resources are firstly allocated for each sub-network with its associated numerology, as they are independent communication systems to each other. Then, the existing solutions for resource allocation are performed for each independent sub-network. Two particular cases of sub-network resource allocation are shown, denoted as parallel and sequential operation modes [27]. The former consists of transmitting the several data streams of each numerology in different portions of frequency resources, following the principle of frequency-division multiplexing (FDM) among the sub-networks. The latter consists of transmitting the different information of each numerology at different time resources, following the principle of time-division multiplexing (TDM) among the sub-networks. More details are provided in the following two sub-sections, where each case has its strengths and weaknesses.

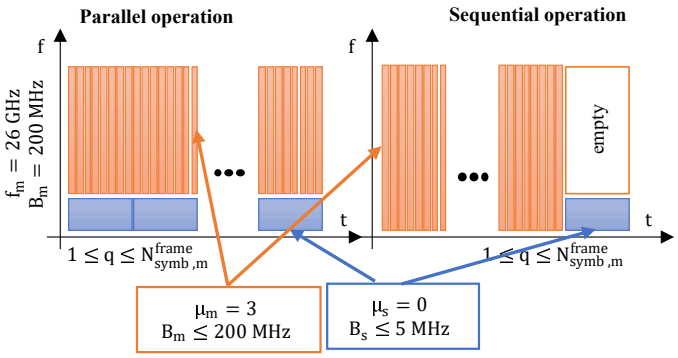

Fig. 5. Example of time-frequency resource allocation for a multi-numerology system. The resource grid of a mmWave system is given for the particular case of $\mu_m = 3$, while the resource grid is for sub-6 GHz is $\mu_s = 0$.

B. The Parallel Operation Mode - FDM

The parallel operation mode allows the simultaneous deployment of the two sub-networks at the same time at different portions of frequency resources, following the FDM principle, see left of Fig. 5. This operation mode will alleviate the complexity of the resource allocation optimization problem since it can be split by two independent resource allocation sub-processes for each sub-network with its corresponding numerology given by a subset of resources in the frequency domain.

The main advantage is that this operation mode will reduce the latency of the system since the UE can access all sub-networks at any moment, thanks to the permanent availability of these sub-networks. This mode is especially tolerant against mobility cases, the narrow beams at mmWave can be exploited for beam-tracking while the wide beams at sub-6 GHz are used to establish a permanent communication link between the micro-BS and UE. However, these benefits also come at the expense of suffering from a range reduction. The deployment of multiple parallel beams towards the UE and the FS-RIS from the micro-BS ($N_B = 2$) will reduce the directivity of each beam and the coverage of the area of interest.

In order to analyze the potential performance of this mode, the number of available resources to be allocated at each sub-network can be computed as

$$\begin{aligned}\mathcal{R}_e=\{\ (k,q)\,,\quad & k_{e,\text{init}}\leq k\leq k_{e,\text{init}}+\frac{B_e}{\Delta f},\\ & 1\leq q\leq N^{\text{frame}}_{\text{symb,max}}\ \}\,,\quad e\in\{m,s\}\,,\end{aligned} \tag{34}$$

where $k_{e,\text{init}}$ is the the first subcarrier index devoted for the e-th sub-network.

C. The Sequential Operation Mode - TDM

In the sequential operation mode, only one sub-network is allowed to be operated for a certain time out of the entire frame, and hence it follows the TDM principle. An illustrative example is depicted in the right part of Fig. 5, the sub-network operated at sub-6 GHz via FS-RIS is activated at the end of the frame, while the sub-network operated at mmWave is enabled for the rest of the frame.

The main advantage of this mode is that the complexity of the resource allocation problem is lower than the parallel one since the micro-BS only has to perform the resource allocation focusing only on a single numerology (sub-network) for a particular time, instead of simultaneously handling different sub-networks operated at several bands as in the parallel operation mode. Additionally, this mode also has a better coverage range, since the micro-BS only needs to deploy one single beam ($N_B = 1$) pointing towards either the FS-RIS at the sub-6GHz or directly to the UE at the mmWave in different periods of resource allocation. However, this mode also possesses two main disadvantages, which are the inefficient exploitation of the resources and the higher latency as compared to the parallel operation mode. The former comes that only one sub-network is available for a specific period, and therefore the huge available bandwidth at the mmWave is not exploited when the sub-6 GHz sub-network is operated.

Again, similarly to the parallel operation mode, the number of available resources of each sub-network for a frame in the sequential mode is given by

$$\mathcal{R}_e = \{\ (k,q)\,, \quad 1 \le k \le \frac{B_e}{\Delta f}, \quad q_{e,\text{init}} \le q \le q_{e,\text{last}}\ \}\,, \quad (35)$$

where $e \in \{m, s\}$, $q_{e,\text{init}}$ and $q_{e,\text{last}}$ denote the first and last OFDM symbol index for the e-th sub-network. Comparing (35) to (34), the sequential operation mode has an additional constraint in the time domain, and hence its potential performance is lower than the parallel one in terms of available resources. A numerical comparison of these operation modes and the combination of them will be given in Section VII.

D. Analysis of the Delay Overhead of the BMP

In this subsection, the delay overhead of the proposed architecture as compared to the existing CoMP [7] is analytically characterized. Following [7], [18], multiple BSs operated at different carrier frequencies that belong to the sub-6 GHz band are assisting the micro-BS operated at mmWave. Hence, the token e can be redefined as $e \in \mathcal{E}$ such that $\mathcal{E} = \{m, s_1, \ldots s_{N_\text{a}}\}$, where N_a is the number of sub-6 GHz carrier frequencies, which are assisting the mmWave cellular network. For the particular case of CoMP, each assisting sub-6 GHz carrier frequency is operated by a macro-BS, however, for the case of the proposed architecture, each sub-6 GHz carrier frequency is obtained by using different FS-RISs.

The required time to perform the beam-sweeping making use of all the codewords of a given codebook at the e-th subnetwork is given by $T_{b,e} \le N_e N_{\text{symb}}^{\text{SSB}} T_{\text{symb},e}$, $e \in \mathcal{E}$, where $N_{\text{symb}}^{\text{SSB}}$ is the number of OFDM symbols required for transmitting an SSB. For the particular case of 5G [1], $N_{\text{symb}}^{\text{SSB}} = 4$ since it is built by the primary synchronization signal (PSS), secondary synchronization signal (SSB) and physical broadcast channel (PBCH).

As a reference case and to show the benefits of the proposed system, the required time for performing the whole BMP of a CoMP system [18] can be modelled as

$$T_{\text{BMP}}^{\text{MP}} = \sum_{e\in\mathcal{E}} \left(\frac{3}{2}T_{b,e} + 2T_{p,e}\right) + \sum_{\substack{e\in\mathcal{E}\\ e\neq m}} T_{d,e}, \quad (36)$$

where $T_{p,e}$ is the propagation time of the signal for the e-th sub-network, which can be computed by using the speed of the light (c) and their corresponding distances to each BS, and it is multiplied by a factor of 2 since it accounts for the SSB transmitted in the DL and the report in the UL. $T_{d,e}$ denotes the delay between the transmission of the information of the UEs from the e-th BS to the following one ($e = s_i \rightarrow s_{i+1}$, $1 \le i < N_a$ or $e = s_{N_a} \rightarrow m$), which includes the networking operation time, processing time at the BS, etc. The duration of $T_{d,e}$ is typically the dominant term according to [18] (5 ms $< T_{p,e} <$ 160 ms), and therefore its value will impose the performance of the overall system. Additionally, note that the sweeping process for each BS ($T_{b,e}$) consists of sweeping the whole 3D space twice, the UE measures the received power of the SSB transmitted at each codeword in the first sweep, and then the UE is reporting its best beam to the BS by using the best codeword in the second sweeping (see Fig. 4). Assuming that the position of the UE is uniformly distributed in the angular space, the average time of this report is half of the sweeping period, and it results in the factor of 3/2.

The required time to perform the whole BMP for the proposed FS-RIS-aided cellular network, described in Fig. 4, can be modelled as

$$\begin{aligned} T_{\text{BMP}}^{\text{FS}} = &\left(\frac{3}{2}T_{b,s_1} + 2T_{p,s_1}\right) \\ &+ \sum_{\substack{e\in\mathcal{E}\\ e\neq s_1}} \left(T_{b,e} + T_{p,e}\right) + \sum_{\substack{e\in\mathcal{E}\\ e\neq m}} \left(T_{\text{symb},e} + T_{p,e}\right). \end{aligned} \quad (37)$$

Comparing (37) to (36), the first term is the same since all UEs must enter the system for the first time by making use of the double beam-sweeping at the lowest carrier frequency (s_1) no matter the chosen architecture. The second term is also the same as in CoMP since one beam-sweeping is required to be performed at each carrier frequency (from s_2 to m) to spread the SSB. However, the third term is different because the beam report can be immediately transmitted after the beam-sweeping by making use of the previous already established sub-network via FS-RIS (from s_1 to s_{N_a}). In the case of exploiting the parallel operation mode, the scheduler must only allocate a UL resource at the previous sub-network to the UE for sending back the beam report after the beam-sweeping process. However, in the sequential operation mode, the scheduler must also consider contiguously allocating the resources in the time domain for performing the beam-sweeping process at the current sub-network and the previous sub-network for reporting. Finally, the delay $T_{d,e}$ is not considered in the

proposed case since only one micro-BS is involved in the BMP. Consequently, the proposed system is more efficient in terms of delay overhead since it has a lower processing time for carrying out all the BMP.

According to [18], the performance of a communication system can be measured as

$$\eta_e = \begin{cases} 1 - T^e_{\text{BMP}}/T_c & \text{if } T^e_{\text{BMP}} < T_c \\ 0 & \text{otherwise} \end{cases}, \quad e \in \{\text{FS}, \text{MP}\} \tag{38}$$

where η_{FS} and η_{MP} are efficiencies of the considered communication systems by taking into account the time devoted to performing the whole BMP and the channel coherence time (T_c) [22], which is the period that the channel remains quasi-static, and it can be computed as $T_c = 0.423/f_D$, where f_D correspond to the maximum Doppler spread. Regarding (38), the proposed FS-RIS system is more efficient than the existing CoMP ($\eta_{\text{FS}} > \eta_{\text{MP}}$) since more data symbols can be transmitted within the coherence period.

The choice of the correct beam (codeword) at each sub-network, especially at the mmWave is not only crucial for communications since it will enhance the signal to noise ratio (SNR), but it also will help to provide accurate position tracking of the UEs thanks to the narrow beams of mmWave. The maximum detectable angular speed at the mmWave for the proposed system relying on FS-RIS and CoMP can be computed as

$$w^e_{\text{max}}\,[\text{rad/s}] \leq \beta \frac{\min\left(\Delta\phi_m, \Delta\theta_m\right)}{T^e_{\text{BMP}}}, \quad Pr\left(\beta\right) = 1 - \beta, \tag{39}$$

respectively, where $e \in \{\text{FS}, \text{MP}\}$, $0 < \beta < 1$ and it is selecting the maximum angular movement from a specific point within the beam-width and $Pr\left(\beta\right)$ denotes the probability of a UE that can be detected by this computed angular speed. Tthe proposed system can detect targets with a higher speed since its BMP period is significantly lower, making the FS-RIS technology more suitable for mobility scenarios.

VII. Performance Evaluation

In this section, several numerical results are provided to show the performance of the proposed FS-RIS, especially the multi-frequency BMP as compared to the existing techniques, such as hierarchical BMP [8]–[10] and CoMP [7]. A summary of the simulation parameters is given in Table I. The default attenuation of the meta-surface is $L_F = 10$ dB. Besides, it is assumed that up to two FS-RISs are involved in the proposed architecture, working at different sub-6 GHz carrier frequencies. For the sake of space, the BMP comparison is only executed in the azimuth dimension, whose angle width of the sector of interest is given by $\Delta\phi_c$, and assuming that the optimum elevation angle is given.

A. Evaluation of the Coverage Range

In Fig. 6, the coverage range of the sub-network operated at the sub-6 GHz band via FS-RIS is given by exploiting different carrier frequencies (f_s), bandwidths (B_s) and attenuations (L_F) for a range of values of distance between the BS↔FS-RIS (d_{bf}). The reference case corresponds to the coverage range

TABLE I
Simulation Parameters

$\mathbf{P_{max}}$	20 dBm	$\mathbf{S_n}$	−174 dB/Hz
$\mathbf{T_{frame}}$	10 ms	γ	3
$\mu_\mathbf{m}$	3	$\mu_\mathbf{s}$	0 & 1
$\mathbf{f_m}$	26 GHz	$\mathbf{f_s}$	800 MHz, 6 GHz
$\mathbf{B_m}$	200 MHz	$\mathbf{B_s}$	5, 10 MHz
$\mathbf{M_B} = \mathbf{M_B^x M_B^y}$	32×32	$\mathbf{M_F} = \mathbf{M_F^x M_F^y}$	64×64

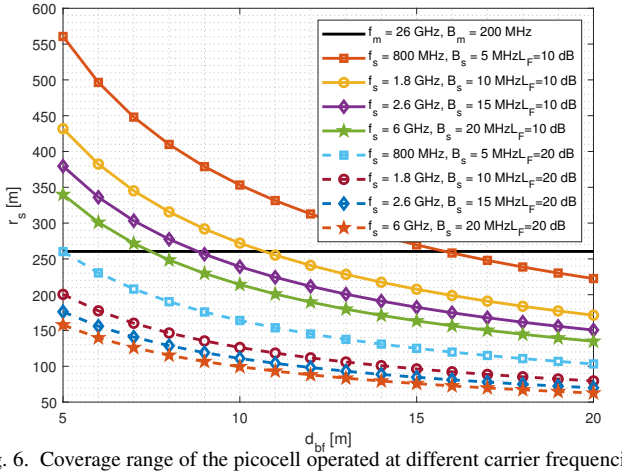

Fig. 6. Coverage range of the picocell operated at different carrier frequencies f_s bandwidths B_s and attenuations (L_F).

provided by the narrow directive beams at the mmWave, whose microcell radio is $r_m \approx 260$ m. Then, the coverage range of different chosen options operated at sub-6 GHz carrier frequencies are also depicted, showing that the distance between the BS↔FS-RIS (d_{bf}) should be reduced as the carrier frequency (f_s) and bandwidth (B_s) are increased to compensate the enhancement of the path-loss and receiver noise. For the particular case of $L_F = 10$ dB (solid lines), the recommended values for the deployment of the FS-RIS concerning the micro-BS is approximated $d_{bf} = \{7 - 16\}$ m to provide the same coverage area as the micro-BS operated at the mmWave. This fact does not only imply that the FS-RIS should be placed closely to the micro-BS, facilitating the set-up process, but it also highlights that the coverage area is not reduced when wider beams are used, unlike the hierarchical BMP [8]–[10]. Then, for the case of $L_F = 20$ dB (dotted lines), the attenuation of the FS-RIS is strongly increased. Due to this additional loss produced by the FS-RIS, its coverage range is significantly reduced as compared to the previous case, and therefore, the FS-RIS is no longer able to provide the same range as the microcell and producing a mismatch among different sub-networks, similarly to the CoMP case [7].

A performance comparison in terms of used codewords and coverage range between the traditional hierarchical BMPs [8]–[10] and the proposed multi-frequency via FS-RIS is given in Tables II and III, respectively. Regarding Table II, the existing hierarchical BMP possesses the lowest latency since it uses the least number of codewords in the BMP, thanks to using beams of different widths at the expense of losing the coverage range. The broader beams are obtained by switching off some elements of the UPA, and hence the directivity is decreased and the microcell radius is reduced from 376 to 56 m. A negative impact will be that those further UEs from the micro-

TABLE II
HIERARCHICAL BMP AT MMWAVE IN THE BS [8]–[10].

$M_x^{BS} \times M_y^{BS}$	Num. used/ total beams	Beamwidth	Directivity	Range
4×4	4/4	26.28°	15 dB	63 m
8×8	2/8	12.78°	18 dB	102 m
16×16	2/16	6.36°	25 dB	163 m
32×32	2/32	3.18°	32 dB	260 m

TABLE III
PROPOSED MULTI-FREQUENCY BMP RELYING ON FS-RISS.

Carrier Freq.	Num. used / total beams	Beamwidth	Directivity	Range
f_s = 800 MHz	4/4	53.36°	8 dB	260 m
f_s = 6 GHz	8/18	6.88°	25 dB	260 m
f_m = 26 GHz	3/38	3.18°	32 dB	260 m

BS are never discovered by the traditional hierarchical BMP. In Table III, the performance of the proposed multi-frequency BMP relying on up to two FS-RISs operated at different sub-6 GHz carrier frequencies is given. The proposed method is also hierarchically oriented, despite it being slightly longer as compared to the hierarchical one, the proposed BMP executed at a lower carrier frequency via FS-RIS has the same range as compared to the BMP executed at the mmWave despite the directivity being lower. The reason behind this advantage is that sub-6 GHz signals not only have a lower attenuation but also have reduced bandwidth which decreases the noise at the receiver. Therefore, the proposed method has the advantage of discovering all the UEs within the sector of the microcell, no matter their distance to either the micro-BS or the FS-RIS.

B. Evaluation of the Overhead Delay

In Fig. 7, a performance comparison in terms of efficiency between the existing CoMP [7] and the proposed FS-RIS-assisted cellular system is given. It is assumed that T_c = 20 ms and the delay is the same between any pair of BSs ($T_d = T_{d,e}, \forall e \in \mathcal{E}$). The efficiency of CoMP rapidly falls to zero as the overhead delay is increased, showing that the impact of the overall system in CoMP strongly depends on the duration of the overhead produced by information transferred among the BS. For the case of two BSs (solid blue), the efficiency is zero when $T_c \approx T_d$, while for the case of three BSs (dotted red), the efficiency is zero when $T_c \approx T_d/2$). On the contrary, the proposed scheme based on FS-RIS does not rely on the overhead delay since its efficiency is a constant function (solid yellow and dotted purple). Additionally, the proposed architecture has a higher performance than the CoMP since the beam report is sent by using an already sub-6 GHz link via FS-RIS, this effect can be seen in the particular case of T_d = 0 ms, where both cases of CoMP is lower than the proposed architecture.

In Fig. 8, a comparison in terms of maximum angular speed between the CoMP [7] and the proposed scheme is also shown for β = 0.5. Again, the proposed system based on FS-RIS can detect those targets with a higher speed than the existing CoMP counterparts, and its detection ability is independent of the overhead delay. The maximum angular speed is extremely sensitive to the delay overhead shown in (39). When the

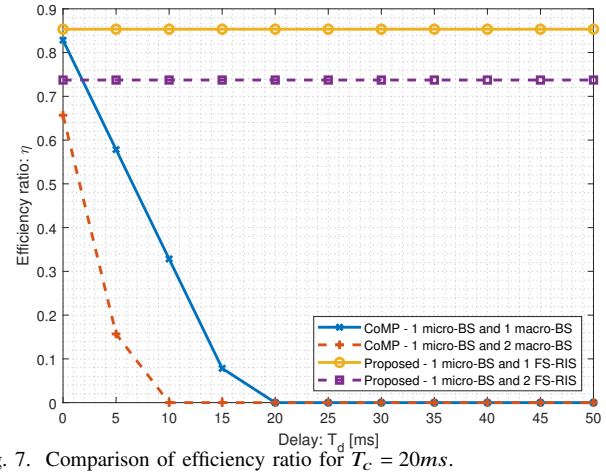

Fig. 7. Comparison of efficiency ratio for $T_c = 20ms$.

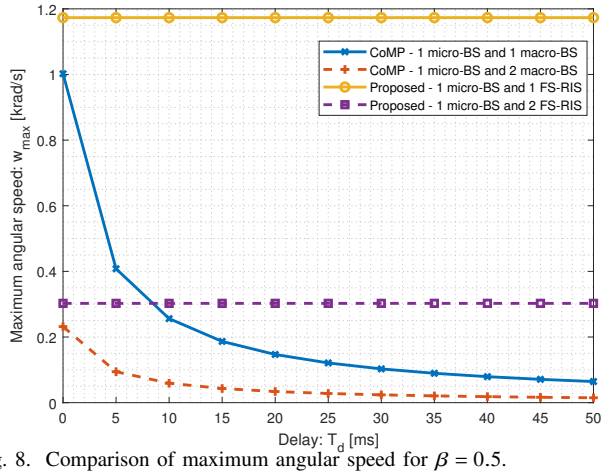

Fig. 8. Comparison of maximum angular speed for $\beta = 0.5$.

number of BSs in CoMP and/or the number of FS-RIS in the proposed system are increased, the angular speed is reduced as the delay overhead is enlarged according to (36) and (37), respectively. On the contrary, the maximum detectable angular speed for the CoMP is significantly degraded by the overhead delay, reducing its capability for providing a communication service to those UEs in motion. Similarly to the case of efficiency given in Fig. 7, even for the case of T_d = 0 ms, the CoMP is still worse than the proposed scheme, since the latter can take advantage of the existing established link at sub-6 GHz band via FS-RIS. Therefore, the proposed scheme relying on FS-RIS is better for supporting high-speed targets.

A comparison between the proposed technique and the standard BMP executed only at mmWave in terms of the number of required codewords (N_c) is given in Fig. 9. In this comparison, the hierarchical BMP [8]–[10] and the CoMP [7] are discarded due to their constraints related to range reduction and excessive overhead delay. The standard BMP relies on using narrow pencil-shape beams at mmWave to thoroughly sweep the whole sector (solid blue), which is the only way to find out all UEs from a single micro-BS. However, the number of required codewords is directly proportional to the width of the sector within the microcell ($\Delta\phi_c$), showing that the incurred latency of the system is again high, especially for large-angle sectors. For the particular case of f_s = 800

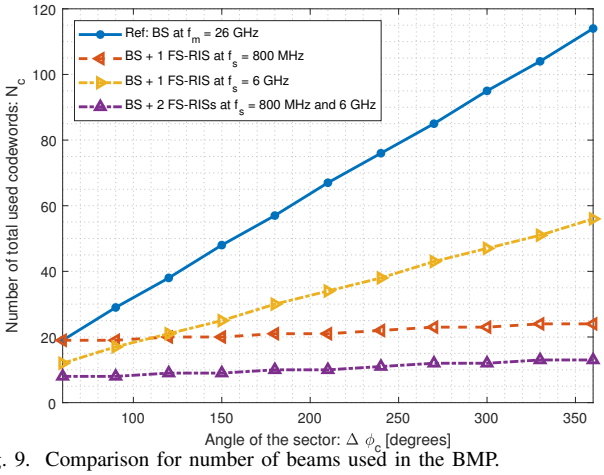

Fig. 9. Comparison for number of beams used in the BMP.

MHz (dashed red), the number of total required codewords is almost constant since the number of required codewords at the first stage (sub-6 GHz) is lower than the second stage (mmWave) ($N_s << N_m$) since their beam widths are 53.36° and 3.18°, respectively. Hence, this setup is convenient for sectors with large dimensions due to the fact that the beam width of the first stage can easily cover the whole space with few codewords. On the other hand, for the case of f_s = 6 GHz (dashed yellow), the total number of required codewords strongly depends on the size of the sector since the beam width of the of the first stage (sub-6 GHz) has significantly reduced (6.88°) and it is comparable to the beam width of the second stage (mmWave). The number of codewords in the first stage is greater than the second one only for large sectors ($N_s >> N_m$), Therefore, this configuration setup is only preferable in small size sectors. Additionally, the combination of using different carrier frequencies operated at sub-6 GHz is significantly better than the reference case since several sizes of beam width can be obtained (dotted lines). It must be remarked that the use of only one FS-RIS is already enough to significantly decrease the number of required codewords to cover the whole space (dotted yellow and red). For the particular case of f_s = 800 MHz (dotted red), the number of necessary codewords is almost constant no matter the size of the sector, especially suitable for larger sectors. Additionally, if two FS-RISs operated at different carrier frequencies are combined (dotted purple), the number of codewords required to perform the BMP is further decreased, which is the best solution.

C. Evaluation of Number of Available RBs at the Two Operation Modes

A comparison in terms of total number and the percentage of available RBs within one frame between the proposed FS-RIS architecture for the two proposed operation modes and the existing CoMP [7] is given in Tables IV and V, respectively. The reference case for this comparison corresponds to the CoMP [7] and its performance is the upper bound (100 %) since all BSs can be simultaneously operated at their respective cells. The results showed that the total number of available resources for the sequential (TDM) and parallel

TABLE IV
NUMBER OF AVAILABLE RBS AT THE TWO OPERATION MODES AS COMPARED TO THE COMP [7].

	N_{RB}^{frame}		
	CoMP	**Sequential (TDM)**	**Parallel (FDM)**
f_s = 800 Mhz	67200	3360	67200
f_s = 6 Ghz	134400	67200	67200
f_m = 26 Ghz	5913600	5322240	5644800
Total	6115200	5332320	5779200

TABLE V
PERCENTAGE OF THE NUMBER OF AVAILABLE RBS AT THE TWO OPERATION MODES AS COMPARED TO THE COMP [7].

	Percentage %		
	CoMP	**Sequential (TDM)**	**Parallel (FDM)**
f_s = 800 Mhz	1.1	0.06	1.1
f_s = 6 Ghz	2.2	0.11	1.1
f_m = 26 Ghz	96.7	87.03	92.31
Total	100	87.2	94.51

(FDM) operation modes are slightly lower than the reference case of CoMP, 5% and 13% respectively. However, the proposed architecture based on FS-RIS does not suffer from the long delay overhead as illustrated before in Fig. 7. Moreover, the energy consumption of the proposed technique is lower than CoMP, since the FS-RIS are fully passive and no radio-frequency chains are required. The impact of the reduction in the number of available RBs of the proposed architecture is minimal since it has many other relevant advantages, such as delay overhead, coverage range, etc. Hence, the proposed FS-RIS is the best solution capable of trading off between the performance of the system and the required resources.

VIII. CONCLUSIONS

A new architecture for mmWave cellular networks relying on the FS-RIS is proposed to deploy high-bandwidth communications under mobility scenarios. The FS-RIS can shift the carrier frequency of the micro-BS from the mmWave to the sub-6 GHz band, thanks to the constant phase variation of each reflecting element at the meta-surface. The sub-6 GHz signals have both lower attenuation and noise power at the receiver, and hence they are crucial to reliably spread the control information of the mmWave network to the whole cell, avoiding the well-known strong blockage and deafness issues present at mmWave. Additionally, it also provides broader beams capable of covering the whole 3D space within a short period, reducing the latency of the system for deploying high-capacity communication under mobility scenarios.

A novel multi-frequency BMP relying on FS-RIS for an mmWave system is given. The combination of multiple beams at different sizes, obtained at each converted carrier frequency via FS-RIS, will simplify the BMP by strongly reducing its execution time. The theoretical analysis and numerical results showed that the performance of the proposed architecture does not suffer a range reduction as compared to the traditional hierarchical BMP, and it has a significantly lower delay than the existing CoMP. Meanwhile, the number of available resources in the proposed architecture, with only one micro-BS, is slightly reduced as compared to CoMP,

which relies on the simultaneous exploitation of multiple BSs. Consequently, the proposed architecture is the best candidate to trade-off between performance and cost, since the FS-RIS are made of low-cost devices and its energy consumption is lower than a regular BS since no radio-frequency chain is required. Consequently, the novel FS-RIS can be implemented in a wireless system and improve the quality of the existing communications. Considering all the benefits of FS-RIS, it will change the paradigm of the current cellular networks and accelerate its evolution to 6G and beyond.

REFERENCES

[1] *5G-NR; Physical channels and modulation (Release 17)*, 3GPP Std. 38.211, 2022.

[2] F. Dong, F. Liu, Y. Cui, W. Wang, K. Han, and Z. Wang, "Sensing as a service in 6G perceptive networks: A unified framework for ISAC resource allocation," *IEEE Trans. Wirel. Commun.*, vol. 22, no. 5, pp. 3522–3536, May 2023.

[3] J. Xu, X. Xia, K.-M. Luk, and W. Hong, "Millimeter-wave array antennas using broadband 3D folded strip elements for B5G/6G communications," *IEEE Trans. Antennas Propag.*, vol. 70, no. 12, pp. 11 569–11 581, Dec. 2022.

[4] M. Zhang, L. Shen, X. Ma, and J. Liu, "Toward 6G-enabled mobile vision analytics for immersive extended reality," *IEEE Wirel. Commun.*, vol. 30, no. 3, pp. 132–138, Jun. 2023.

[5] H. S. Ghadikolaei, "MAC aspects of millimeter-wave cellular networks," in *Wireless Mesh Networks*. Rijeka: IntechOpen, 2019, ch. 7.

[6] R. Congiu, H. Shokri-Ghadikolaei, C. Fischione, and F. Santucci, "On the relay-fallback tradeoff in millimeter wave wireless system," in *IEEE INFOCOM Workshops*, Apr. 2016, pp. 622–627.

[7] H. Shokri-Ghadikolaei, C. Fischione, G. Fodor, P. Popovski, and M. Zorzi, "Millimeter wave cellular networks: A MAC layer perspective," *IEEE Trans. Commun.*, vol. 63, no. 10, pp. 3437–3458, Oct. 2015.

[8] H. Zhou, D. Guo, and M. L. Honig, "Beam acquisition and training in millimeter wave networks with narrowband pilots," *IEEE J. Sel. Areas Commun.*, vol. 37, no. 12, pp. 2759–2771, Dec. 2019.

[9] J. Wang, W. Tang, S. Jin, C.-K. Wen, X. Li, and X. Hou, "Hierarchical codebook-based beam training for RIS-assisted mmwave communication systems," *IEEE Trans. Commun.*, vol. 71, no. 6, pp. 3650–3662, Jun. 2023.

[10] C. You, B. Zheng, and R. Zhang, "Fast beam training for IRS-assisted multiuser communications," *IEEE Wireless Commun. Lett.*, vol. 9, no. 11, pp. 1845–1849, Nov. 2020.

[11] K. Chen-Hu, G. C. Alexandropoulos, and A. g. Armada, "Differential data-aided beam training for RIS-empowered multi-antenna communications," *IEEE Access*, vol. 10, pp. 113 200–113 213, Oct. 2022.

[12] W. Yan, W. Hao, C. Huang, G. Sun, O. Muta, H. Gacanin, and C. Yuen, "Beamforming analysis and design for wideband THz reconfigurable intelligent surface communications," *IEEE J. Sel. Areas Commun.*, vol. 41, no. 8, pp. 2306–2320, Aug. 2023.

[13] C. Pan, G. Zhou, K. Zhi, S. Hong, T. Wu, Y. Pan, H. Ren, M. D. Renzo, A. Lee Swindlehurst, R. Zhang, and A. Y. Zhang, "An overview of signal processing techniques for RIS/IRS-aided wireless systems," *IEEE J. Sel. Top. Signal Process.*, vol. 16, no. 5, pp. 883–917, Aug. 2022.

[14] K. Zhi, C. Pan, H. Ren, K. K. Chai, and M. Elkashlan, "Active RIS versus passive RIS: Which is superior with the same power budget?" *IEEE Commun. Lett.*, vol. 26, no. 5, pp. 1150–1154, May 2022.

[15] A. Shaltout, A. Kildishev, and V. Shalaev, "Time-varying metasurfaces and lorentz non-reciprocity," *Opt. Mater. Express*, vol. 5, no. 11, pp. 2459–2467, Nov. 2015.

[16] L. Zhang, X. Q. Chen, S. Liu, Q. Zhang, J. Zhao, J. Y. Dai, G. D. Bai, X. Wan, Q. Cheng, G. Castaldi, V. Galdi, and T. J. Cui, "Space-time-coding digital metasurfaces," in *Metamaterials*, Sep. 2019, pp. 128–130.

[17] J. C. Ke, J. Y. Dai, J. W. Zhang, Z. Chen, M. Z. Chen, Y. Lu, L. Zhang, L. Wang, Q. Y. Zhou, L. Li, J. S. Ding, Q. Cheng, and T. J. Cui, "Frequency-modulated continuous waves controlled by space-time-coding metasurface with nonlinearly periodic phases," *Light: Science & Applications*, vol. 11, no. 273, Sep. 2022.

[18] P. Xia, C.-H. Liu, and J. G. Andrews, "Downlink coordinated multi-point with overhead modeling in heterogeneous cellular networks," *IEEE Trans. Wirel. Commun.*, vol. 12, no. 8, pp. 4025–4037, Aug. 2013.

[19] J. Yuan, E. De Carvalho, R. J. Williams, E. Björnson, and P. Popovski, "Frequency-mixing intelligent reflecting surfaces for nonlinear wireless propagation," *IEEE Wirel. Commun. Lett.*, vol. 10, no. 8, pp. 1672–1676, Aug. 2021.

[20] Y. Ra'di, N. Nefedkin, P. Popovski, and A. Alù, "Metasurfaces for next-generation wireless communication systems," *National Science Review*, vol. 10, no. 8, 05 2023.

[21] *Study on channel model for frequencies from 0.5 to 100 GHz (Release 17)*, 3GPP Std. 38.901, 2022.

[22] T. Rappaport, *Wireless communications: Principles and practice*, 2nd ed. Prentice Hall, 2002.

[23] J. Xu, S.-J. Lee, W.-S. Kang, and J.-S. Seo, "Adaptive resource allocation for MIMO-OFDM based wireless multicast systems," *IEEE Trans. Broadcast.*, vol. 56, no. 1, pp. 98–102, Mar. 2010.

[24] Y. Zhang and C. Leung, "Resource allocation in an OFDM-based cognitive radio system," *IEEE Trans. Commun.*, vol. 57, no. 7, pp. 1928–1931, Jul. 2009.

[25] L.-H. Shen, P.-Y. Wu, and K.-T. Feng, "Energy efficient resource allocation for multinumerology enabled hybrid services in b5g wireless mobile networks," *IEEE Trans.Wirel. Commun.*, vol. 22, no. 3, pp. 1712–1729, Mar. 2023.

[26] L.-H. Shen, C.-Y. Su, and K.-T. Feng, "Comp enhanced subcarrier and power allocation for multi-numerology based 5G-NR networks," *IEEE Trans. Veh. Technol.*, vol. 71, no. 5, pp. 5460–5476, May 2022.

[27] K. Sehla, T. M. T. Nguyen, G. Pujolle, and P. B. Velloso, "Resource allocation modes in C-V2X: From LTE-V2Xto 5G-V2X," *IEEE Internet Things J.*, vol. 9, no. 11, pp. 8291–8314, Jun. 2022.

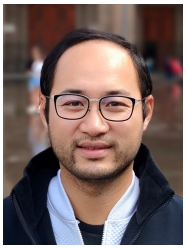

Kun Chen-Hu (S'16-GS'20-M'21) received his Ph.D. degree in Multimedia and Communications in 2019 from Universidad Carlos III de Madrid (Spain). Currently, he is a post-doctoral researcher in Aalborg University (Denmark). He was awarded by UC3M in 2019 in recognition of his outstanding professional career after graduation. He visited Eurecom (France) and Vodafone Chair TU Dresden (Germany), both as guest researcher. He also participated in different research projects in collaboration with several top companies in the area of mobile communications. He was the Web Chair for Globecom 2021 and MeditCom 2024, Madrid (Spain), and online content editor for IEEE ComSoc. His research interests are related to signal processing techniques, such as waveforms design, reconfigurable intelligent surfaces, non-coherent massive MIMO and channel estimation.

Robin J. Williams received his M.Sc. in Wireless Communications in 2019 from Aalborg University, Denmark. He is currently a Ph.D. fellow at Department of Electronic Systems, Aalborg University, Denmark. His research interests include electromagnetic modelling, multiple-input multiple-output systems, and reflective intelligent surfaces.

Andrea Alù (Fellow, IEEE) is a Distinguished Professor at the City University of New York (CUNY), the Founding Director of the Photonics Initiative at the CUNY Advanced Science Research Center, the Einstein Professor of Physics at the CUNY Graduate Center, Professor of Electrical Engineering at the City College of New York, Senior Research Scientist and Adjunct Professor at the University of Texas at Austin. He received the Laurea, MS and PhD degrees from the University of Roma Tre, Rome, Italy, respectively in 2001, 2003 and 2007. After performing postdoctoral research at the University of Pennsylvania, in 2009 he joined the faculty of the University of Texas at Austin, where he was the Temple Foundation Endowed Professor until 2018. In 2015 he was the Royal Netherlands Academy of Arts and Sciences (KNAW) Visiting Professor at the AMOLF Institute in the Netherlands.

His research interests cover metamaterials and metasurfaces, applied electromagnetics, optics, nanophotonics, and acoustics. He is currently the Editor-in-Chief of Optical Materials Express and has been serving on the Editorial Board of Reviews of Electromagnetics, Physical Review B, Advanced Optical Materials, Laser and Photonics Reviews, New Journal of Physics, EPJ Applied Metamaterials and ISTE Metamaterials. He served as Associate Editor for IEEE Antennas and Wireless Propagation Letters, Optics Express, Applied Physics Letters, MDPI Materials, Scientific Reports, Metamaterials, and Advanced Electromagnetics. He has guest edited special issues for the IEEE Journal of Selected Topics in Quantum Electronics, Proceedings of IEEE (twice), IEEE Transactions on Antennas and Propagation, IEEE Antennas and Wireless Propagation Letters (twice), Nanophotonics, Journal of Optics, Journal of the Optical Society of America A and B, Photonics and Nanostructures - Fundamentals and Applications, Optics Communications, Metamaterials, and Sensors on a variety of topics involving metamaterials, plasmonics, optics and electromagnetic theory.

Petar Popovski (Fellow, IEEE) is a Professor at Aalborg University, where he heads the section on Connectivity and a Visiting Excellence Chair at the University of Bremen. He received his Dipl.-Ing and M. Sc. degrees in communication engineering from the University of Sts. Cyril and Methodius in Skopje and the Ph.D. degree from Aalborg University in 2005. He received an ERC Consolidator Grant (2015), the Danish Elite Researcher award (2016), IEEE Fred W. Ellersick prize (2016), IEEE Stephen O. Rice prize (2018), Technical Achievement Award from the IEEE Technical Committee on Smart Grid Communications (2019), the Danish Telecommunication Prize (2020) and Villum Investigator Grant (2021). He was a Member at Large at the Board of Governors in IEEE Communication Society 2019-2021. He is currently an Editor-in-Chief of IEEE JOURNAL ON SELECTED AREAS IN COMMUNICATIONS and a Chair of the IEEE Communication Theory Technical Committee. Prof. Popovski was the General Chair for IEEE SmartGridComm 2018 and IEEE Communication Theory Workshop 2019. His research interests are in the area of wireless communication and communication theory. He authored the book "Wireless Connectivity: An Intuitive and Fundamental Guide".